Entropy growth during free expansion of an ideal gas

Subhadip Chakraborti[1], Abhishek Dhar[1], Sheldon Goldstein[2], Anupam Kundu[1] and Joel L. Lebowitz[2]
[1] *International Centre for Theoretical Sciences, Tata Institute of Fundamental Research, Bengaluru 560089, India and*
[2] *Departments of Mathematics and Physics, Hill Center, Rutgers, The State University of New Jersey, 110 Frelinghuysen Road, Piscataway, New Jersey 08854-8019, USA*

(Dated: December 26, 2021)

To illustrate Boltzmann's construction of an entropy function that is defined for a microstate of a macroscopic system, we present here the simple example of the free expansion of a one dimensional gas of non-interacting point particles. The construction requires one to define macrostates, corresponding to macroscopic variables. We define a macrostate M by specifying the fraction of particles in rectangular boxes $\Delta x \Delta v$ of the single particle position-velocity space $\{x, v\}$. We verify that when the number of particles is large the Boltzmann entropy, $S_B(t)$, of a typical microstate of a nonequilibrium ensemble coincides with the Gibbs entropy of the coarse-grained time-evolved one-particle distribution associated with this ensemble. $S_B(t)$ approaches its maximum possible value for the dynamical evolution of the given initial state. The rate of approach depends on the size of Δv in the definition of the macrostate, going to zero at any fixed time t when $\Delta v \to 0$. Surprisingly the different curves $S_B(t)$ collapse when time is scaled with Δv as: $t \sim \tau/\Delta v$. We find an explicit expression for $S_B(\tau)$ in the limit $\Delta v \to 0$. We also consider a different, more hydrodynamical, definition of macrostates for which $S_B(t)$ is monotone increasing, unlike the previous one which has small decaying oscillations near its maximum value. Our system is non-ergodic, non-chaotic and non-interacting; our results thus illustrate that these concepts are not as relevant as sometimes claimed, for observing macroscopic irreversibility and entropy increase. Rather, the notions of initial conditions, typicality, large numbers and coarse-graining are the important factors. We demonstrate these ideas through extensive simulations as well as analytic results.

I. INTRODUCTION

According to the second law of thermodynamics, any spontaneous change in an isolated system leads to an increase of the thermodynamic entropy, S (as defined by Clausius). The second law thus provides in a sense an arrow of time and quantifies the irreversibility that we observe in everyday physical phenomena. Understanding how such irreversibility emerges from the microscopic reversible Newtonian dynamics of a many-particle system was the remarkable achievement of Boltzmann. He pointed out the key idea that the observed irreversibility is the typical macroscopic behaviour given appropriate initial conditions, that becomes a certainty when we take the system size truly macroscopic. Boltzmann also provided a clear prescription for the construction of an entropy function (which we denote as S_B) that is defined for a *single* microstate of a macroscopic system in a given macrostate. This entropy function is defined for a system in or out of equilibrium. It is equal to the thermodynamic entropy for a system in equilibrium.

The deep and somewhat subtle ideas of Boltzmann [1] have been widely discussed [2–5] and clarified in recent work [6–9]. We mention here a particularly relevant quote from Ref. [10]: *Time-asymmetric behavior as embodied in the second law of thermodynamics is observed in individual macroscopic systems. It can be understood as arising naturally from time-symmetric microscopic laws when account is taken of a) the great disparity between microscopic and macroscopic sizes, b) initial conditions, and c) that what we observe are "typical" behaviors — not all imaginable ones. Common alternate explanations, such as those based on equating irreversible macroscopic behavior with ergodic or mixing properties of ensembles (probability distributions) already present for chaotic dynamical systems having only a few degrees of freedom or on the impossibility of having a truly isolated system, are either unnecessary, misguided or misleading.*

The present work is an attempt to provide a numerical demonstration of some of the above ideas presented in [9] through a simple example.

Our microscopic model is a gas of $N(\gg 1)$ non-interacting point particles of unit masses confined to move inside a one-dimensional box of length L. Initially the gas is in thermal equilibrium (to be defined more precisely later) and confined, by a partitioning wall, to the left half of the box. We consider its subsequent evolution on removal of the partition. In our work we consider two distinct (families of) macroscopic variables. For the first, we consider a coarse graining of the single particle phase space $\{\mu \equiv (x, v)\}$ into rectangles Δ_μ with volumes $\Delta x \Delta v$ and look at the distribution $f(x, v, t)$ of particles in this space. This leads to a definition of S_B, that we refer to as S_B^f. The second macroscopic description is given by the three locally conserved fields $U = \{\rho(x,t), p(x,t), e(x,t)\}$ corresponding to mass, momentum and energy — defined using a spatial coarse-graining. The Boltzmann entropy corresponding to U will be referred to as S_B^U.

We study the time evolution of the two choices of macrovariables, f and U, and the associated entropies, S_B^f, S_B^U. The simplicity of the model allows us to perform highly accurate simulations with large number of particles (of order 10^7) and compute both mean distributions (averaged over initial ensembles) analytically as well as empirical ones (with single realizations).

We find that as expected, both S_B^f and S_B^U approach for long times their equilibrium values with the behaviour of a typical macrostate being the same as that averaged over the initial ensemble. There are however some interesting surprises in the time evolution of $S_B^f(t)$. The rate at which $S_B^f(t)$ increases depends strongly on Δv with $dS_B^f(t)/dt$ apparently going to zero as $\Delta v \to 0$. However, upon rescaling time, $t \to \tau/\Delta v$, the different curves collapse to a single curve $S_B^f(\tau)$. This curve has small decaying oscillations near its maximum. We obtain an analytic expression for $S_B^f(\tau)$ which agrees with the observations. There are no such surprises for $S_B^U(t)$ which increase monotonically to the equilibrium value.

We point to some of the earlier studies related to this issue. The evolution of Boltzmann's entropy has earlier been investigated numerically in interacting systems such as fluid models [11–14], in systems evolving via maps [15]. Some subtleties for dense fluids were pointed out by Jaynes in [16], discussed further in [17] and numerically investigated in [18]. The one dimensional gas of equal mass hard point particles and hard rods was extensively studied earlier as one of the tractable models where dynamical properties can be obtained analytically and where the question of entropy increase has been investigated. Some of the interesting questions addressed concern dynamical correlations and the evolution of the single particle distribution function [19–25]. The Euler hydrodynamic equations for the hard rod system were first obtained in [26] and have more recently been discussed in [27] as an example of an interacting integrable model, where it is also shown that there are dissipative Navier-Stokes corrections which vanish when one goes from rods to point particles. The effect of integrability-breaking on entropy growth was studied in [28] for hard rods in a harmonic trap. Boltzmann's ideas also appear in recent discussions of thermalization in isolated quantum systems [29, 30]. In contrast to these earlier studies, the present work considers the case of a completely non-interacting system, namely the ideal gas in one dimension.

The plan of the paper is as follows. In Sec. II we define the Boltzmann entropy for a general classical macroscopic system. We then describe the precise model, the different definitions of entropy that are studied and the choices of macrostates. In Sec. III we present our numerical results on the evolution of the macroscopic fields and the entropy functions for the two different choices of macrovariables. This section also contains the derivation of the expression for $S_B^f(\tau)$ in the rescaled time τ. For s_B^U, we present an analysis of the results based on the "hydrodynamic" equations for the macroscopic fields. In Sec. IV we study how these macrovariables and the associated (Boltzmann) entropies evolve with time for atypical initial conditions. A geometric picture of the dynamics in phase space is provided in Sec. V and we conclude with a discussion in Sec. VI. Some exact results for the evolution of the macroscopic fields are presented in App. A.

II. BOLTZMANN'S ENTROPY, DEFINITION OF THE MICROSCOPIC MODEL AND CHOICE OF MACROSTATES

A. Boltzmann's entropy

The microstate of a classical system of N particles of unit mass confined in a box, denoted by X, is specified by the positions $\mathbf{x}_i$ and velocities $\mathbf{v}_i = \mathbf{p}_i$, with $i = 1, 2, ..., N$, *i.e.*, $X = (\mathbf{x}_1, \mathbf{x}_2, \ldots \mathbf{x}_N, \mathbf{v}_1, \mathbf{v}_2, \ldots, \mathbf{v}_N)$. The dynamics of the system is given by a Hamiltonian $H(X)$.

We now consider a macroscopic or "coarse-grained" description for the case $N \gg 1$. A simple example of such a description is provided by the macrovariable $N_{\rm left}$ which gives the total number of particles in the left half of the box. Clearly, this is a function of the microstate X and we can write $N_{\rm left}(t) = M(X(t))$, with $M(X) = N_{\rm left}(X)$.

In general we can describe a macrostate by specifying a set of macrovariables $M(X) = \{M_1(X), M_2(X), ..., M_n(X)\}$, with resolution $\Delta M = \{\Delta M_j\}$ [9]. We identify these macrostates with the elements of a partition of the full phase space Γ into sets $\Gamma_{\hat{M}}$ of the form

$$\Gamma_{\hat{M}} = \{X \in \Gamma | \hat{M}_j \le M_j(X) \le \hat{M}_j + \Delta M_j, j = 1, ..., n\}. \tag{1}$$

These provide a coarse-grained description in the sense that many different X correspond to the same range of values of the macrovariable $M(X)$, and hence to the same set $\Gamma_{\hat{M}}$.

Each microstate X belongs to some set $\Gamma_{\hat{M}}$ corresponding to the coarse-grained value of the macrovariable $\hat{M} = \hat{M}(X)$ (thus for $X \in \Gamma_{\hat{M}}$ as in Eq. (1), $\hat{M}(X) = \hat{M}$). Boltzmann's insight was to associate to each microscopic state X an entropy, through the set $\Gamma_{\hat{M}}$ to which it belongs [6, 8, 9, 31]:

$$S_B(X) = S_B[\hat{M}(X)] = \ln |\Gamma_{\hat{M}}|, \tag{2}$$

where we have set Boltzmann's constant $k_B = 1$. The volume of the set $\Gamma_{\hat{M}}$ is

$$|\Gamma_{\hat{M}}| = \int \prod_{i=1}^{N} d\mathbf{x}_i d\mathbf{p}_i \; \mathbb{1}[X \in \Gamma_{\hat{M}}], \tag{3}$$

where $\mathbb{1}$ represents the indicator function. As the system evolves under the Hamiltonian dynamics, the microstate is given by $X(t)$ while the macrovariable evolves as $M(t) = M(X(t))$. Consequently the corresponding set $\Gamma_{\hat{M}}(t) = \Gamma_{\hat{M}(X(t))}$ also evolves, thereby specifying the time evolution of the Boltzmann entropy as $S_B(t) = S_B[\Gamma_{\hat{M}}(t)]$. Boltzmann argued that for an isolated system starting from a microstate corresponding to a low entropy $S_B(0)$, the system evolves in such a way that $S_B(t)$ "typically" increases for macroscopic sys-

tems even though the microscopic evolution is completely time-reversal symmetric. (In what follows we shall drop the hats on the macrovariables, slightly abusing notation.)

Among all possible macrostates of a system there are two very important ones: the equilibrium macrostate M_{eq} and the initial macrostate $M_{\rm ini}$. The entropy of the initial macrostate $S_B(t=0) = S_B(M_{\rm ini})$ is low by assumption. On the other hand, the macro-region $\Gamma_{M_{eq}}$ is overwhelmingly large compared to other macro-regions associated to other macrostates. It is so large that it contains most of the phase space volume of Γ_E, an energy shell, assumed to contain all the macrostates M. More precisely, for large N, the ratio of their volumes $|\Gamma_{M_{eq}}|/|\Gamma_E| \approx 1 - e^{-cN}$ where c is a positive constant [31–33]. This property corresponds to equilibrium because the system should stay in (or near) $\Gamma_{M_{eq}}$ for long times, consistent with the observed stationarity in thermodynamic equilibrium.

Since $\Gamma_{M_{\rm eq}}$ takes up almost all the volume of Γ_E, when the system starts from a microstate X belonging to a non-equilibrium macrostate $M_{\rm ini}$ such that $S_B(M_{\rm ini}) < S_B(M_{\rm eq})$, its microscopic dynamics should 'typically' take the microstate to regions Γ_M of larger phase space volume and thus of larger entropy S_B and eventually to $\Gamma_{M_{\rm eq}}$, unless the dynamics given by the Hamiltonian has strong constraints, for example additional conservation laws, or the initial state X is very special [34]. Hence we expect the quantity $S_B(M)$ to increase for the majority (in fact the overwhelming majority) of microstates in $\Gamma_{M_{\rm ini}}$ except for a few whose total volume relative to $|\Gamma_{M_{\rm ini}}|$ goes to zero in the $N \to \infty$ limit. Because of this expectation one can make direct connection between $S_B(M_{\rm eq})$ and S (the thermodynamic entropy) in an equilibrium state as suggested by Boltzmann. For an isolated system in equilibrium with energy E, volume V and N particles [8]

$$S(E,V,N) \simeq S_B(M_{\rm eq}(E,V,N)), \quad \text{for large } N. \tag{4}$$

We briefly comment here on why Gibbs' definition of entropy cannot be used in the nonequilibrium situation. We recall first that the Gibbs entropy of an equilibrium canonical ensemble $\varrho_{\rm eq}$ is defined as

$$S_G[\varrho_{\rm eq}(X)] = -\int \prod_{i=1}^{N} dx_i dp_i \;\; \varrho_{\rm eq}(X) \;\; \ln \varrho_{\rm eq}(X), \tag{5}$$

and this can be identified for macroscopic systems with the thermodynamic entropy S. Extending this definition to the non-equilibrium situation described by an evolving ensemble $\varrho_t(X)$ one obtains the corresponding Gibbs entropy $S_G(t) = S_G[\varrho_t(X)]$. However, we note that the volume preserving dynamics is described by the Liouville equation

$$\partial\varrho/\partial t = \{H, \varrho\}. \tag{6}$$

This ensures that this entropy does not change with time, i.e., $dS_G(t)/dt = 0$.

A general study of the Boltzmann entropy and the coarse grained Gibbs entropy, related to the F_α in Eq. (11), is given in Chapters IV and V of Ref. [35]. The discussions there are enlightening. Another book with a clear analysis of the issues discussed in this article is by Oono [36].

B. Definition of the model and choices of macrostates

Our model consists of N non-interacting point particles of mass 1 confined in a one dimensional box of size L. The Hamiltonian of the system $H = \sum_{j=1}^{N} v_j^2/2$ consists of only kinetic energy. In between collisions with the walls (at $x = 0, L$), each particle moves at constant velocity. On collisions with the walls, the velocities are reversed.

We now describe the two families of macrovariables that we will consider in this study.

Choice I — The distribution of particles in the single-particle phase space: We consider μ-space $\{(x,v)\}$ and divide it into cells Δ_α, each of size $|\Delta_\alpha| = \Delta x \Delta v$. For a given microstate $X = \{x_i, v_i\}$ we specify the number of particles N_α in each cell. We then obtain the particle number density in each cell:

$$f_\alpha = \frac{N_\alpha}{|\Delta_\alpha|}. \tag{7}$$

This satisfies the normalization $\sum_\alpha f_\alpha |\Delta_\alpha| = N$. The set $\{f_\alpha\}$ specifies our first family of macrovariables, with its corresponding macrostates. The "number" of microstates (volume) for a given specification of $\{N_\alpha\}$ is given by $|\Gamma_M| = \prod_\alpha [|\Delta_\alpha|^{N_\alpha}/N_\alpha!]$. Thus, with $S_B^f = \ln|\Gamma_M|$, we have using Stirling's formula for large N the entropy per particle

$$s_B^f = S_B^f/N = -\frac{1}{N}\sum_\alpha |\Delta_\alpha| f_\alpha \ln f_\alpha, \tag{8}$$

up to an additive constant.

To get a handle on the behavior of s_B^f we also consider, for a finite number of particles, an average over initial microscopic configurations chosen from a phase space distribution $\varrho_0(\{x_i, v_i\})$:

$$F(x,v,t) = \sum_{i=1}^{N} \langle \delta(x_i - x)\delta(v_i - v)\rangle \,, \tag{9}$$

which we note is the single-particle marginal obtained from the full phase space density $\varrho_t(\{x_i, v_i\})$ with initial distribution ϱ_0. For our ideal gas, $F(x,v,t)$ obeys the autonomous equation

$$\partial_t F + v\partial_x F = 0, \tag{10}$$

and can be computed analytically as shown in App. A. We can now define a coarse-grained distribution corre-

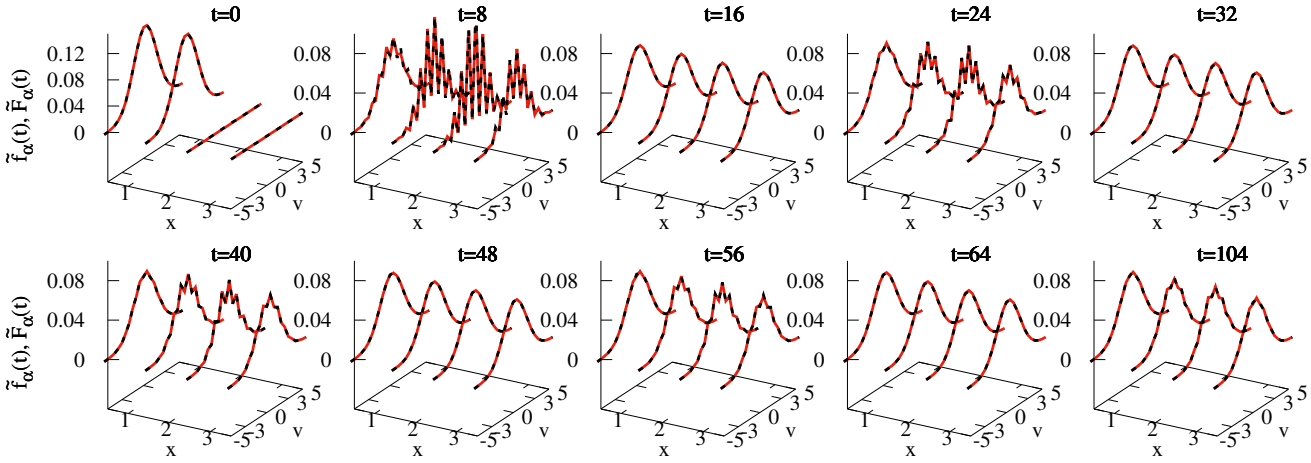

FIG. 1. Plot of evolution of the empirical particle density $\tilde{f}_\alpha(t) = f_\alpha(t)/N$ (black dashed lines) starting from a single initial microscopic configuration in the two-dimensional μ-space for grid size $\Delta x = \Delta v = 0.5$ and $N = 10^7$, $L = 4$. In the single initial configuration, the positions of the particles are distributed uniformly between $(0, L/2)$ and the velocities are drawn from the Maxwell distribution given by Eq. (16) with canonical temperature $T_0 = 2.5$. We observe that $\tilde{f}_\alpha(t)$ approaches towards its equilibrium form at large times, however the convergence is oscillatory as can be seen from the recurrences at times $t = 16,\ 32,\ 48,\ 64$ to very close to the equilibrium form. The evolution is also compared with the analytical result for the averaged single particle distribution $\tilde{F}_\alpha = F_\alpha(t)/N$ from Eqs. (11) and (A8) which is obtained after averaging over initial configurations chosen from uniform position distribution over $(0, L/2)$ and Maxwell velocity distribution at temperature $T_0 = 2.5$ (this is the equilibrium state in the left half of the box). The good agreement between $\tilde{f}_\alpha(t)$ and $\tilde{F}_\alpha(t)$ is a consequence of typicality.

sponding to a partition of the μ-space as

$$F_\alpha = \frac{1}{|\Delta_\alpha|}\int_{x,v\in\Delta_\alpha} dx\ dv F(x,v,t), \tag{11}$$

and a corresponding coarse-grained entropy:

$$s^F_\Delta = -\frac{1}{N}\sum_\alpha |\Delta_\alpha| F_\alpha \ln F_\alpha. \tag{12}$$

Note that this has a similar form to Eq. (8); however, here we have used mean distributions instead of the empirical distributions used there. These will in fact typically be more or less the same, a consequence of the law of large numbers.

We note that if we let $|\Delta_\alpha| \to 0$ in Eqs. (11) and (12) then for any fixed t,

$$s^F_\Delta \to s^F = -\frac{1}{N}\int dx dv F \ln F, \tag{13}$$

which, since the evolution of F satisfies Eq. (10), makes s^F independent of t . This would also be the case for s^f_B when $\Delta_\alpha \to 0$, $N \to \infty$, and f_α is suitably normalized. This is due to the fact that we are dealing with a non-interacting system so that s^F is just, up to normalization, the Gibbs entropy of the entire N-particle system (whose distribution can be taken to be the evolving product of F's), which does not change under the time evolution. We shall see later that even for the ideal gas if we look on a time scale proportional to $1/\Delta v$ we will see $s^F_\Delta \approx s^f_B$ increase with time albeit non-monotonically.

Choice II - The spatial distribution of mass, momentum and energy: We divide the box $(0, L)$ into K cells δ_a, $a = 1, 2...K$, each of size $\ell = L/K$. For a given microscopic configuration X, let N_a be the number of particles in cell δ_a and let P_a and E_a be the total momentum and total energy of these particles. In this case the macrostate is defined by these set of locally conserved quantities $U = \{N_a, P_a, E_a\}$ and we obtain the Boltzmann entropy $S^U_B = \ln|\Gamma_U|$ where $|\Gamma_U|$ is the volume of the phase space region Γ_U corresponding to the macrostate U. For large N this entropy per particle attains the form

$$s^U_B = \frac{S^U_B}{N} = \frac{1}{N}\sum_a \rho_a \ell\ s(\rho_a, \epsilon_a), \tag{14}$$

where $s(\rho_a, \epsilon_a)$ is the ideal gas entropy per particle for density $\rho_a = N_a/\ell$ and internal energy density $\epsilon_a = [E_a - P_a^2/(2N_a)]/\ell = e_a - p_a^2/(2\rho_a)$, with $p_a = P_a/\ell, e_a = E_a/\ell$ being the momentum density and total energy density respectively. This is given explicitly (up to additive constant terms) by:

$$s(\rho,\epsilon) = -\ln\rho + \frac{1}{2}\ln\left(\frac{\epsilon}{\rho}\right)\ . \tag{15}$$

III. RESULTS FOR THE TIME EVOLUTION OF MACROSTATES AND ENTROPY INCREASE

A. Choice I of the macrovariables

1. *Numerical results*

We consider $N = 10^7$ particles initially uniformly distributed in the left half $(0, L/2)$ of the box with box size $L = 4$. For our non-interacting point particle system, the choice of system size L is inconsequential and hence we arbitrarily set $L = 4$. Since we keep the system length fixed, changing N corresponds to changing the density in our system. There is no upper bound to the density since there is no effective interaction between the particles. In real systems the number of particles would scale with the volume. The initial velocities of our microstate are drawn from the Maxwell distribution given by

$$g_{\rm eq}(v, T_0) = \left(\frac{1}{2\pi T_0}\right)^{1/2} \exp\left(-\frac{v^2}{2T_0}\right), \qquad (16)$$

with temperature $T_0 = 2.5$. This is the canonical ensemble corresponding to the equilibrium macrostate with particles in the left half of the box. We thus choose a *single random realization* from this canonical ensemble as our initial microstate. Equivalently we can choose the initial configuration from a microcanonical ensemble with total energy $E = NT_0/2$. The region $\Gamma_{M_{\rm ini}}$ then consists of all $X \in \Gamma_E$ such that $N_{\rm left}(X) = N$.

We divide the μ-space (x-v space) of the system into grids of size $\Delta_\alpha = \Delta x \Delta v$ and calculate the evolution of the empirical single particle density f_α given by Eq. (7) by performing microscopic simulations of the evolution of the given microstate. In Fig. (1) we plot $\tilde{f}_\alpha = f_\alpha(t)/N$ at different points x_α, v_α in μ-space and at different times, for $\Delta x = \Delta v = 0.5$. We observe that $\tilde{f}_\alpha(t)$ approaches its equilibrium form non-monotonically in time with near-recurrences to the equilibrium distribution. At large times, the $\tilde{f}_\alpha(t)$ finally reaches the equilibrium form where particles are uniformly distributed between $(0, L)$ and velocities are Maxwellian with temperature $T_0 = 2.5$. We also compare the empirical $\tilde{f}_\alpha(t)$ (black dashed lines) and mean distribution $\tilde{F}_\alpha(t) = F_\alpha(t)/N$ (red solid lines), calculated for the same grid size, at different times. The mean distribution $F_\alpha(t)$ is computed analytically from Eqs. (11) and (A8). We find good agreement between the empirical density $\tilde{f}_\alpha(t)$ and the mean distribution $\tilde{F}_\alpha(t)$ — a consequence of the typicality implied by the law of large numbers for this non-interacting model. We have verified that this agreement is also valid when we choose the initial random configuration from a microcanonical distribution with energy per particle given by $T_0/2$.

In Fig. (2) we show the evolution of the corresponding entropy $s_B^f(t)$ [given by Eq. (8), where we fix the additive constant so that at $t = 0$, this agrees with Eqs. (14,15)] during free expansion, for the same random single realization and parameters as in Fig. (1). We plot $s_B^f(t)$

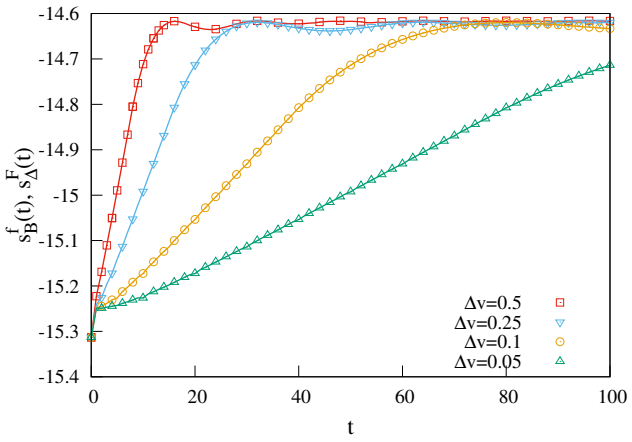

FIG. 2. Top figure: A comparison between $s_B^f(t)$ obtained from simulation of a single realization, and $s_\Delta^F(t)$ obtained after an ensemble average, plotted as a function of time during free expansion. For evaluating $s_B^f(t)$ we use the same single initial condition used in Fig. (1) for $N = 10^7$ in a box of size $L = 4$. We compute $s_B^f(t)$ for different grid sizes $|\Delta_\alpha| = \Delta x \Delta v$ by keeping $\Delta x = 0.5$ fixed and varying $\Delta v = 0.5$ (red empty squares), 0.25 (blue empty inverted triangles), 0.1 (yellow empty circles), and 0.05 (green empty triangles). The solid lines are $s_\Delta^F(t)$ obtained analytically from Eq. (12) for $T_0 = 2.5$. We again observe excellent agreement between $s_B^f(t)$ and $s_\Delta^F(t)$ and notice that they both eventually increase and saturate to the equilibrium value. However the approach to this equilibrium value is oscillatory with decaying amplitude and period $2L/\Delta v$. Also note that the growth rate at any given time decreases with decreasing Δv.

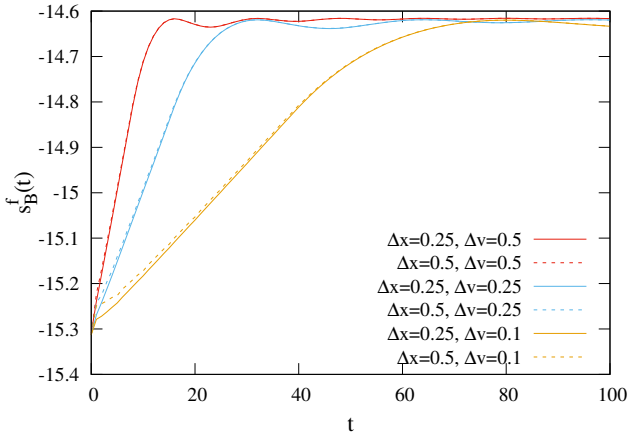

FIG. 3. Plot showing the dependence of growth of the entropy, $s_B^f(t)$, for different spatial resolutions Δx. For any given Δv we find that there is a weak dependence on the size of Δx at early times. The parameter values and initial conditions are the same as in Fig. (1).

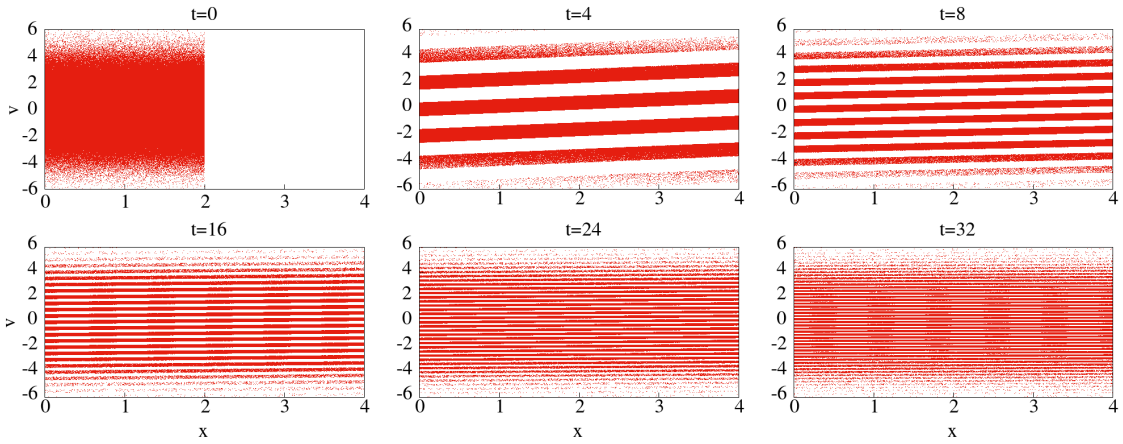

FIG. 4. Plot showing the distribution of $N = 10^6$ particles in the (x, v) plane at different instants of time. These results correspond to a single realization of the time-evolution of the system, for the same parameters and initial conditions as used in Fig. (1).

for different grid sizes by keeping Δx fixed and varying Δv. The solid lines correspond to the entropy $s^F_\Delta(t)$ [given by Eq. (12)] calculated from the exact expression for the mean distribution $F(x, v, t)$. We observe that there is very good agreement between s^f_B and s^F_Δ, as expected. Both the entropies grow, initially monotonically with time, touching a value slightly above the final equilibrium value and then exhibit small oscillations in time with a period $\tau_p = 2L/\Delta v$; these eventually die and the entropy saturates to its equilibrium value. Note that these oscillations were also seen in the recurrences in Fig. (1) and we will discuss their origin in the next subsection.

Though the final increase of entropy appears to be always equal to ln(2), we observe in Fig. (2) that the entropy growth rate decreases with decreasing Δv. In other words, at any fixed time, with decreasing Δv one observes a correspondingly lower entropy. On the other hand we see in Fig. (3) that the entropy growth rate shows convergence on decreasing Δx. This can be understood from the plot of the μ-space distribution shown in Fig. (4). We see that with time, the system keeps developing more and more structure in the velocity direction, while, in the spatial direction it becomes more or less homogeneous after some time. Thus, decreasing the grid size Δx does not give us more information about the system, while decreasing Δv does.

To understand the dependence of s^f_B on Δv consider the limit of vanishing grid size. For large N, corresponding to f_α defined for a given microstate $X = \{x_i, v_i\}$, one can define a smooth function $f(x, v, t)$ such that $N_\alpha = \int_{x,v\in\Delta_\alpha} dxdvf(x, v, t)$ and $\int dxdvf(x, v, t) = N$. The Eq. (8) then becomes

$$s^f_B(t) \approx -\frac{1}{N}\int dx\ dv\ f(x, v, t) \ln f(x, v, t), \quad (17)$$

up to an additive constant. In the large N, small grid size limit, the function $\tilde{f} = \lim_{\Delta x\to 0,\Delta v\to 0} \lim_{N\to\infty} f/N$ satisfies the equation

$$\partial_t \tilde{f} + v\partial_x \tilde{f} = 0, \quad (18)$$

using which it follows that its associated "entropy"

$$\mathcal{s}^f_B(t) = -\int dx\ dv\ \tilde{f}(x, v, t) \ln \tilde{f}(x, v, t), \quad (19)$$

obeys $d\mathcal{s}^f_B(t)/dt = 0$. Thus it would seem that there is no entropy increase in the large N, $\Delta_\alpha \to 0$ limit. However, as is apparent from the numerical findings in Sec. III, for any fixed grid size $|\Delta_\alpha|$ the exact s^f_B, or its approximation on the right hand side of Eq. (8), will typically increase (if initially its value is not at its maximum) over time. For N large and $|\Delta_\alpha|$ small, significant increase may not begin for a very long time (the time at which $\tilde{f}(x, v, t)$ develops structure on the scale $|\Delta_\alpha|$), a reflection of the fact that the entropy in Eq. (19) does not change with time.

The situation is different for a gas of hard spheres of diameter a in 3D where in the Boltzmann-Grad limit, $a \to 0, N \to \infty$ with $Na^2 \to b > 0$, one can define the macrostate by a smooth one-particle empirical density which satisfies the Boltzmann equation, given by Eq. (18) modified by collision terms on the right [3, 37]. As shown by Boltzmann's H-theorem, this leads to increase of the entropy $\mathcal{s}^f_B$.

2. *Scaling analysis for the evolution of entropy*

We now return to the question of the observed oscillation period $\tau_p = 2L/\Delta v$ in Fig. (2). This is easiest to understand once we consider a mapping of the dynamics of particles in a box of length L to the dynamics on a circle of length $2L$. This mapping corresponds to the μ-

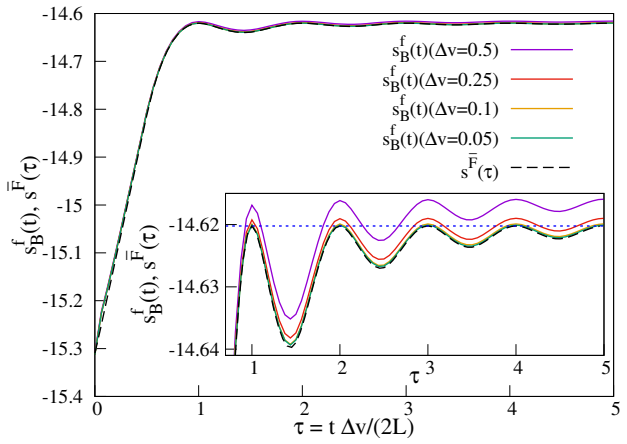

FIG. 5. This figure shows a collapse of the data presented in Fig. (2) for different values of Δv, on plotting the entropy as a function of the scaled time $\tau = t\Delta v/(2L)$. The dashed curve is the analytic prediction from Eq. (20) Inset: A zoom up of the plot. The horizontal dotted line corresponds to the entropy given by the right hand side of Eq. (17) with $f = \rho_0 g_{\rm eq}$, where $\rho_0 = N/L$ and $g_{\rm eq}$ is in Eq. (16). The small overshoot (of s^f_B) that we see for larger Δv arises since a coarse-grained velocity distribution is effectively broader than the Maxwellian from which it comes, leading to a larger effective temperature.

space map ϕ taking $[0, L]\times\mathbb{R}$ to $[0, 2L]\times[0, \infty)$ and given by $(x, v) \to (x, v)$ for $v > 0$ and $(x, v) \to (2L - x, -v)$ for $v < 0$. With this mapping we see that two particles, initially at the same spatial point but with velocity difference Δv (size of the velocity grid), will meet again (possibly in different locations) at times $n\tau_p$, where n is an integer. Furthermore, at the times $t = n\tau_p$, all points that are initially within a cell $\Delta x\Delta v$ will lie on a narrow strip that winds around precisely n times around the circle and still within Δv [see Fig. (6)]. Thus, the spatial distribution of points becomes exactly uniform within the region v to $(v + \Delta v)$ at the times $t = n\tau_p$ and this explains the fact that s^F_Δ (in Eq. (12)) reaches its maximum value at these times. At intermediate times, the winding on the circle is incomplete and we get a lower entropy.

In Fig. (5) we show plots of the entropy time-evolution data for different values of Δv [from Fig. (2)] as a function of the scaled time $\tau = t\Delta v/(2L) \equiv t/\tau_p$. We find a remarkable collapse of the data to a single curve. The physical picture in the preceeding para in fact leads to an analytical understanding of this and we can obtain an explicit expression for the evolution of the entropy in the scaled time variable — this is given by the function:

$$s^{\bar F}(\tau) = -\ln\rho_0 + \frac{1}{2}\ln\frac{T}{2} - \frac{1}{2}\int_0^2 dz R(z,\tau)\ln R(z,\tau), \tag{20}$$

where $\rho_0 = N/L$ and $R(z, \tau)$ is known explicitly (see below); the integral above can be numerically computed. In Fig. (5) we find excellent agreement betwen the collapsed data and the analytic result.

We now present the details of our analytic understanding of the observed scaling and of Eq. (20). For this we use the mapping between the dynamics with reflecting boundary conditions and the dynamics in a periodic box. The dynamics on the circle simply consists of rotations at constant positive velocities which implies $F(x, v, t) = F(x - vt, v, 0)$ [with F periodic in x with period $2L$]. We claim that the following space averaged distribution function will in fact capture the evolution of the entropy of the system at the rescaled time $\tau = t\Delta v/(2L)$:

$$\bar F(x, v, \tau) = \frac{1}{2L\tau}\int_0^{2L\tau} dx' F(x - x', v, 0). \tag{21}$$

We define a corresponding Gibbs entropy per particle:

$$s^{\bar F}(\tau) = -\frac{1}{N}\int_0^{2L} dx \int_0^\infty dv\ \bar F \ln \bar F. \tag{22}$$

More precisely we now show that in the limit $\Delta x \to 0, \Delta v \to 0$, we get

$$\lim_{\Delta\to 0} s^F_\Delta(2L\tau/\Delta v) = s^{\bar F}(\tau), \tag{23}$$

which explains the observed scaling. With the system defined on the circle let us consider the averaged distributions:

$$\begin{aligned}
&F_\alpha(\Delta x, \Delta v)\\
&= \frac{1}{\Delta x\Delta v}\int_{x_\alpha}^{x_\alpha+\Delta x} dx' \int_{v_\alpha}^{v_\alpha+\Delta v} dv' F(x', v', t) &(24)\\
&= \frac{1}{\Delta x\Delta v}\int_{x_\alpha}^{x_\alpha+\Delta x} dx' \int_{v_\alpha}^{v_\alpha+\Delta v} dv' F(x' - v't, v', 0)\\
&\approx = \frac{1}{\Delta v}\int_{v_\alpha}^{v_\alpha+\Delta v} dv' F(x_\alpha - v't, v_\alpha, 0)\\
&= \frac{1}{t\Delta v}\int_0^{t\Delta v} dx' F(x_\alpha - v_\alpha t - x', v_\alpha, 0), &(25)\\
&= \bar F(x_\alpha - v_\alpha t, v_\alpha, t; \tau). &(26)
\end{aligned}$$

Since x is on the circle, we have for small Δx and small Δv,

$$\begin{aligned}
&s^F_\Delta(t) = -\frac{1}{N}\sum_\alpha |\Delta_\alpha| \bar F(x_\alpha - v_\alpha t, v_\alpha, \tau)\ln \bar F(x_\alpha - v_\alpha t, v_\alpha, \tau)\\
&\approx -\frac{1}{N}\sum_\alpha \int_0^{2L} dx \Delta v \bar F(x - v_\alpha t, v_\alpha, \tau)\ln \bar F(x - v_\alpha t, v_\alpha, \tau)\\
&= -\frac{1}{N}\sum_\alpha \int_0^{2L} dx \Delta v \bar F(x, v_\alpha, \tau)\ln \bar F(x, v_\alpha, \tau)\\
&\approx -\frac{1}{N}\int_0^{2L} dx \int_0^\infty dv \bar F(x, v, \tau)\ln \bar F(x, v, \tau)\\
&= s^{\bar F}(\tau), &(27)
\end{aligned}$$

where we used the translational invariance in going from the second to the third step. We note that this result explains the main observations in Fig. (5), namely slowly decaying oscillatory approach to the final value, with precise returns at integer values of τ. Since F has period $2L$, we can write it in the form $F(x,v,0) = \rho_0 \bar{g}(v) + \phi(x,v,0)$ where ρ_0 is the average density in the original box, $\bar{g}(v) = \rho_0^{-1} \int_0^{2L} dx F(x,v,0)/(2L)$ is the averaged global velocity distribution [$\bar{g}$ is normalized to 1/2 on $v > 0$] while $\phi(x,v,0)$ has period $2L$ and mean zero (i.e. $\int_0^{2L} dx \phi(x,v,0) = 0$). Hence clearly $\psi(x,v,\tau) = \int_0^{2L\tau} dx' \phi(x-x',v,0)/(2L)$ is periodic in τ with period 1. Then we have from Eq. (21) that

$$\bar{F}(x,v,\tau) = \rho_0 \bar{g}(v) + \frac{\psi(x,v,\tau)}{\tau}. \tag{28}$$

We see that for integer values of $\tau = 1,2,3,\ldots$, $\bar{F}$ attains the value $\rho_0 \bar{g}(v)$, which yields the time-maximum of the entropy $s^{\bar{F}}$ given by:

$$\begin{aligned} s^{\bar{F}}_{\max} &= -\frac{1}{N} \int_0^{2L} dx \int_0^{\infty} dv \rho_0 \bar{g}(v) \ln[\rho_0 \bar{g}(v)] \\ &= -\ln \rho_0 - 2 \int_0^{\infty} dv \bar{g}(v) \ln[\bar{g}(v)]. \end{aligned} \tag{29}$$

We also see that the deviations of $\bar{F}$, from the value $\rho_0 \bar{g}(v)$, that occur at values of τ between these integers are at most of order $1/\tau$, implying that the same thing is true for the entropy.

For the special initial condition $F(x,v,0) = \rho_0[1 + a\cos(\pi x/L)]h(v)\theta(v)$, with $h(v)$ any even velocity distribution, we get $\bar{F}(x,v,\tau) = \rho_0\{1 - a[\sin[\pi(x/L - 2\tau)] - \sin[\pi x/L]]/(2\pi\tau)\}h(v)$. We thus explicitly find here that $\bar{F} = \rho_0 h(v)$ for $\tau = 1,2,3,...$, with $1/\tau$ deviations for intermediate values as described above. In particular $\bar{F}$ approaches $\rho_0 h(v)$ as $\tau \to \infty$.

Next, we consider the case discussed in Sec. (III A) where the gas is initially confined on the left half of the box. The initial distribution considered is of the product form $F(x,v,0) = \rho(x) g_{\rm eq}(v)\theta(v)$ and we then get:

$$\bar{F}(x,v,\tau = g_{\rm eq}(v)\theta(v) \frac{1}{2L\tau} \int_0^{2L\tau} dx' \rho_c(x-x'), \tag{30}$$

where $\rho_c(x)$ is the initial density profile on the circle $[0,2L]$, given by $\rho_c(x) = 2\rho_0$ for $x \in [0, L/2] \cup [3L/2, 2L]$ and zero elsewhere. To perform the above integral, we Fourier-decompose the density profile as $\rho_c(x) = \sum_{n=-\infty}^{\infty} a_n e^{in\pi x/L}$, where $a_n = (2L)^{-1} \int_0^{2L} \rho_c(x) e^{-in\pi x/L}$. Hence we obtain:

$$\bar{F}(x,v,\tau) = g_{\rm eq}(v)\theta(v) \left[\rho_0 + \sum_{n\neq 0} \frac{a_n e^{in\pi(x/L - \tau)} \sin(n\pi\tau)}{n\pi\tau} \right]. \tag{31}$$

For our initial condition with a half-filled box one finds $a_n = 2\rho_0 \sin(n\pi/2)/(n\pi)$ for $n \neq 0$. Hence we get

$$\bar{F}(x,v,\tau) = g_{\rm eq}(v)\theta(v)\rho_0 R(x/L,\tau), \quad \text{where} \tag{32}$$

$$R(z,\tau) = \left[1 + \frac{4}{\pi^2 \tau} \sum_{n=1}^{\infty} \frac{\cos[n\pi(z-\tau)] \sin(n\pi/2) \sin(n\pi\tau)}{n^2} \right]. \tag{33}$$

The product form of $\bar{F}$ leads to simplifications for the entropy given by Eq. (22) and, we finally obtain Eq. (20) [after fixing additive constants so that at $t = 0$, it agrees with Eqs. (14,15)].

B. Choice II of the macrovariables

1. *Numerical results*

We again start from a typical single realization with $N = 10^7$, $L = 4$ and $T_0 = 2.5$ (the same as that used in Fig. (1)). In this case we partition the box into $K = 40$ cells each of size $\ell = L/40 = 0.1$ and calculate the corresponding empirical density $\rho(x,t)$, velocity $v(x,t) = p(x,t)/\rho(x,t)$ and energy $e(x,t)$ fields. Suppressing the time dependence, we have that $\rho_a = \rho(x_a), p_a = p(x_a)$, and $e_a = e(x_a)$, $x_a \in \delta_a$, with corresponding temperature field $T(x) = 2e(x)/\rho(x) - v^2(x)$. In Fig. (7), we plot these fields at different times. The solid lines are the analytically obtained averaged fields $\bar{\rho}$, $\bar{v}$, and $\bar{T}$ given by Eqs. (A9), (A11), (A13). The details of the analytical calculation of mean fields are provided in App. A. We find excellent agreement between the empirical and mean densities, as expected. We also find that at long times these fields converge to their equilibrium values given by the uniform fields $\rho(x) = \rho_0$, $v(x) = 0$ and $T(x) = T_0$. Unlike for the case of the f-macrovariable, here we do not see an oscillatory approach to the equilibrium state. In fact from the analytic results (see App. A) one can see that the approach to equilibrium at long times takes the form $A(x,t) - A_{\rm eq}(x) \sim B(x)\, e^{-at^2}$ with $a = T_0\pi^2/(2L^2)$, where $A(x,t)$ can be any of the three fields ρ, v, T discussed above, $A_{\rm eq}(x)$ represents its equilibrium value and $B(x)$ is some real known function. Next, we compute the empirical density field for different values of N. In Fig. (8) we plot the evolution of $\rho(x,t)$ for the different values of N and compare them with the respective mean profiles $\bar{\rho}(x,t)$ at different times (black dot-dashed lines). We notice that the empirical density shows fluctuations for small N which decrease for increasing N, leading to better agreement of the empirical profiles with the averaged ones.

We next insert these three fields into Eqs. (14) and (15) to obtain the intensive empirical entropy $s_B^U(t)$. In Fig. (9) we plot $s_B^U(t)$ with time t for different cell sizes ℓ. The solid lines correspond to theoretical computation of $s_B^U(t)$ using the analytical expressions of the mean fields $\bar{\rho}(x,t)$, $\bar{p}(x,t)$ and $\bar{e}(x,t)$ given in App. A. In this case we see that the increase of $s_B^U(t)$ is monotonic and the

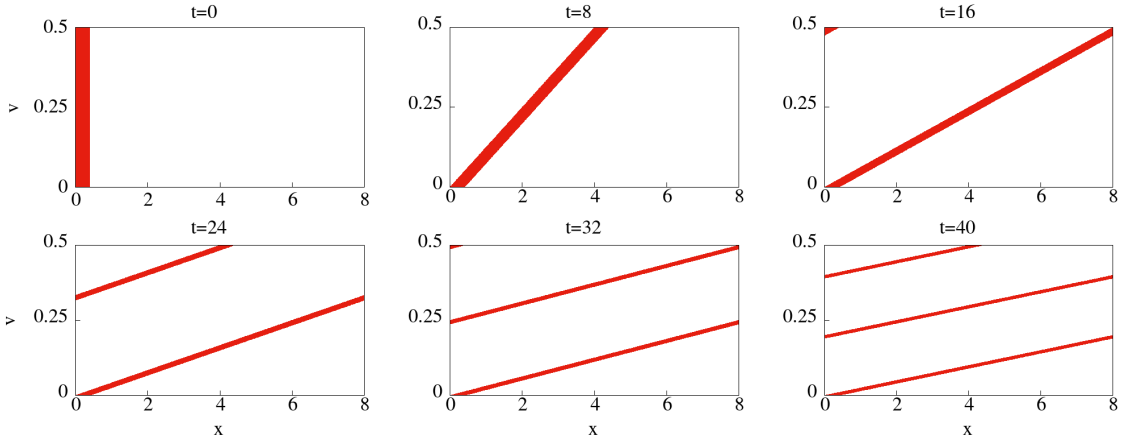

FIG. 6. Plot showing the evolution of $N = 10^5$ particles, in the (x, v) plane, where the particles move on a circle of length $2L = 8$. The particles were initially distributed uniformly in a small box with $\Delta x = 0.25, \Delta v = 0.5$. With time the box gets continually stretched and, at times that are multiples of $2L/\Delta v = 16$, the stretched pieces wind completely around the box. Comparing with Fig. (2) we see that the dips in $s_B^f(t)$ occur at times $\approx 24, 40$, at which the winding around the length $2L$ is complete.

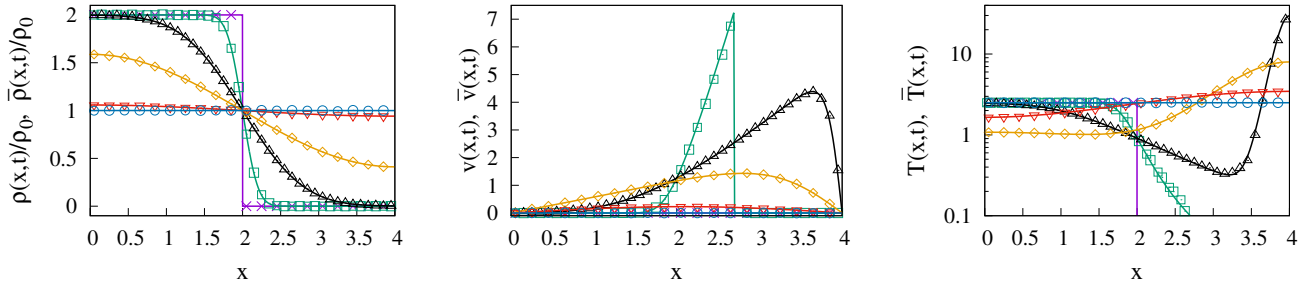

FIG. 7. Plot of the 'typical' spatial profiles of the three conserved fields density $\rho(x,t)$, velocity $v(x,t)$, and temperature $T(x,t)$ at different times $t = 0$ (magenta crosses), 0.1 (green empty squares), 0.4 (black empty triangles), 1 (yellow empty diamonds), 2 (red inverted empty triangles), and 4 (blue empty circles) obtained from simulation of a single configuration with $N = 10^7$ particles. The density is normalised by the mean value $\rho_0 = N/L$. Initial configuration is one realization of the canonical ensemble for particles in the left half $(0, L/2)$ with $L = 4$. The initial positions of the particles are distributed uniformly between $(0, L/2)$ and the initial velocities are drawn from Maxwell distribution given by Eq. (16) with canonical temperature $T_0 = 2.5$. The solid lines are analytically obtained fields $\bar{\rho}, \bar{v} = \bar{p}/\bar{\rho}$, and $\bar{T}$ given by Eqs. (A9), (A11), (A13) (see App. A for details). The excellent agreement between the empirical densities and the mean densities once again establish typicality.

entropy growth rate converges as we decrease the cell size ℓ. The final increase of entropy is again equal to $\ln(2)$, as expected.

2. *Entropy increase for S_B^U and hydrodynamics*

We now explore the connection between the increase of the entropy S_B^U and the behavior of the U-macrovariables in the hydrodynamic limit. It is believed that the Euler equations for the three conserved fields describe, in a suitable regime, the hydrodynamics of a one-dimensional fluid of interacting particles. At the level of the Euler equations there is no entropy increase. While this is well known, we provide an argument for it here, since we will need to refer to the argument later. So consider the one-dimensional Euler equations:

$$\partial_t \rho + \partial_x(\rho v) = 0, \tag{34a}$$

$$\partial_t(\rho v) + \partial_x(\rho v^2 + P) = 0, \tag{34b}$$

$$\partial_t\left(\rho\tilde{e} + \frac{1}{2}\rho v^2\right) + \partial_x\left[v\left(\rho\tilde{e} + \frac{1}{2}\rho v^2 + P\right)\right] = 0, \tag{34c}$$

where $\tilde{e}(x,t) = e/\rho - v^2/2$ (note: ϵ is the internal energy density and $\tilde{e} = \epsilon/\rho$) is the internal energy per particle and the pressure, for an ideal gas system is given by $P =$

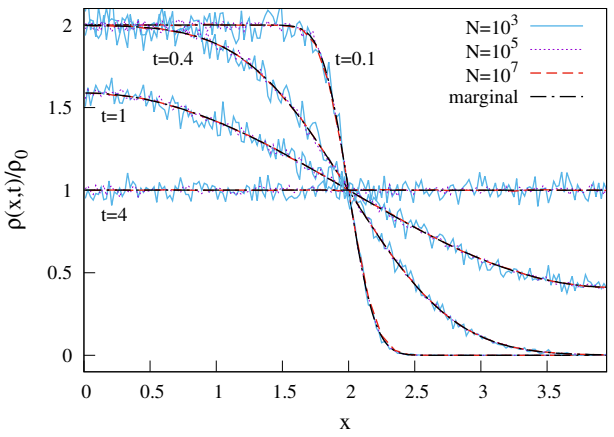

FIG. 8. Testing the dependence of typicality on the number of particles N. We plot the empirical density $\rho(x,t)$ (normalised by $\rho_0 = N/L$) for different N and at different times, along with the mean density. The agreement of the empirical profiles with the averaged ones (dashed-dotted lines) becomes better as N is increased.

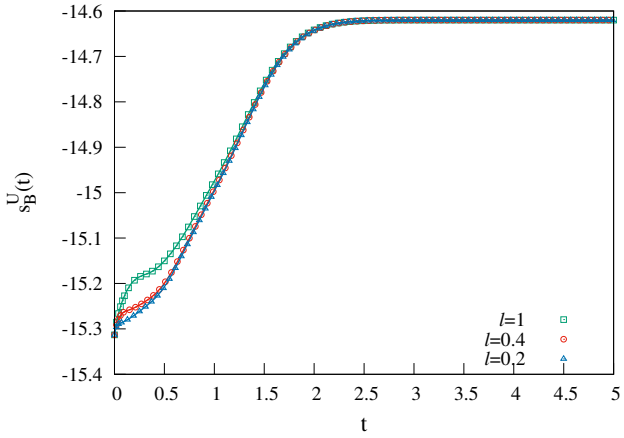

FIG. 9. Plot of entropy per particle, s_B^U, as a function of time during free expansion. Parameter values are: $L = 4, N = 10^5, T = 2.5$. We consider the same single initial configuration as in Fig. (1). The different plots correspond to partitions of size $\ell = 0.2, 0.4, 1$. Unlike in Fig. (2), here we see a monotonic increase and a convergence of the growth rate on decreasing ℓ. The solid lines correspond to the mean field analytic profiles and we find very good agreement with the entropy computed from the empirical fields.

ρT. These equations can be written in the form

$$\frac{D\rho}{Dt} + \rho\partial_x v = 0, \tag{35a}$$

$$\frac{Dv}{Dt} + \frac{1}{\rho}\partial_x P = 0, \tag{35b}$$

$$\frac{D\tilde{e}}{Dt} + \frac{1}{\rho}P\partial_x v = 0, \tag{35c}$$

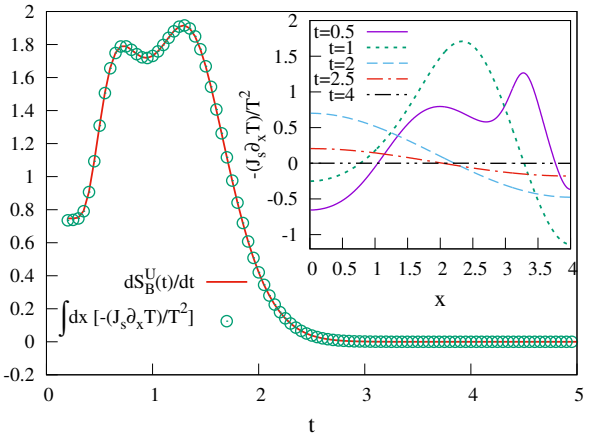

FIG. 10. Verification of entropy production rate as in Fig. (9) using Eq. (40). The red line is the LHS of Eq. (40) where $S_B^U(t)$ is calculated from the definition given by Eq. (14) and the green points are the RHS of Eq. (40) calculated from hydrodynamics. Inset: Plot of the integrand in Eq. (40) with space x at different times.

where $D/Dt = \partial_t + v\partial_x$ denotes the advective derivative. Now we use the Euler hydrodynamic equations along with Clausius' laws of thermodynamics to determine the entropy production rate in the slowly evolving local equilibrium state. Clausius' laws of thermodynamics provide a well-known thermodynamic relation for the ideal gas, given by $TdS = d\tilde{E} + PdL$, where S is the Clausius entropy, $\tilde{E}$ is total internal energy and L is the volume. Applying this relation to a small volume ℓ with a fixed number of particles n_ℓ we find, after some manipulations,

$$Tds = d\tilde{e} + Pd(\ell/n_\ell),$$
$$\text{hence, } \frac{Ds}{Dt} = \frac{1}{T}\left[\frac{D\tilde{e}}{Dt} - \frac{P}{\rho^2}\frac{D\rho}{Dt}\right],$$

with $s(x,t)$ being the entropy per particle. From Eqs. (35a) and (35c) we then immediately obtain that $\frac{Ds}{Dt} = 0$. The total entropy $S(t) = \int_0^L \rho s(x,t)\, dx$ also remains constant, since $dS/dt = -\int_0^L dx\ \partial_x(\rho v s) = 0$, using the boundary conditions $v(0,t) = v(L,t) = 0$. The standard mechanisms of entropy growth in the hydrodynamic description are either additional dissipative (Navier-Stokes-Fourier) terms or the formation of shocks.

We now discuss entropy production in our non-interacting gas using a similar description, keeping in mind that we now do not expect a closed set of hydrodynamic equations with the three fields. In fact it is easy to see that the first two Euler equations in Eqs. (34) continue to hold while the equation for the energy field $e(x,t)$ no longer holds. Formally the energy field satisfies

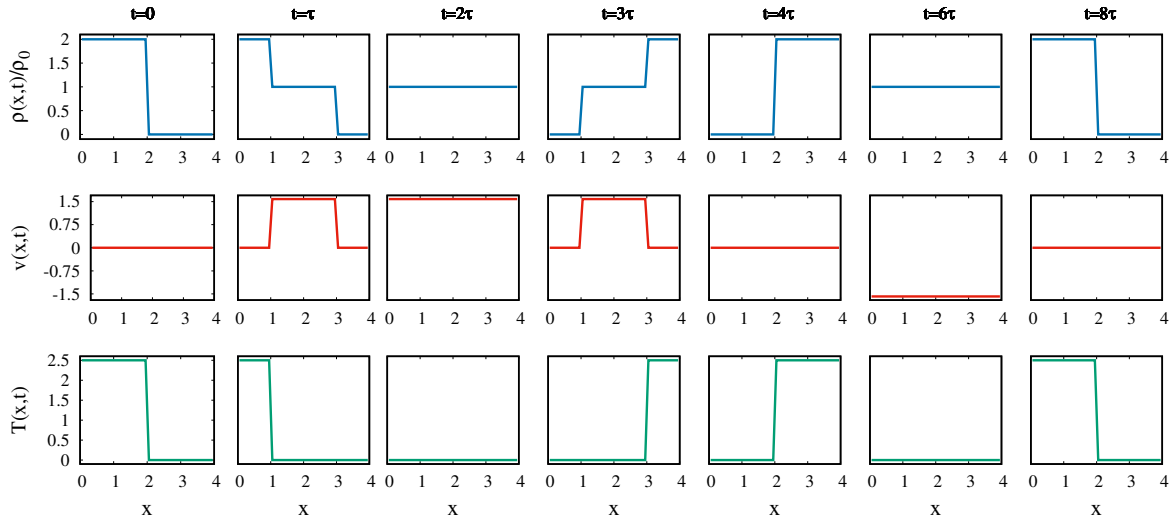

FIG. 11. Plot of the 'atypical' spatial profiles of the three conserved fields density $\rho(x,t)$, velocity $v(x,t)$, and temperature $T(x,t)$ at different times obtained from simulation of a single configuration with $N = 10^7$ particles. The initial positions of the particles are distributed uniformly between $(0, L/2)$ with $L = 4$, and the initial velocities of odd particles are set $v_0 = \sqrt{T_0}$ and of even particles are set $v_0 = -\sqrt{T_0}$, with $T_0 = 2.5$. The profiles repeat themselves after a time period 8τ with $\tau = L/(4\sqrt{T_0})$ and thus the system does not reach an equilibrium at large time in this 'atypical' case. We have used grid size $\ell = 0.1$.

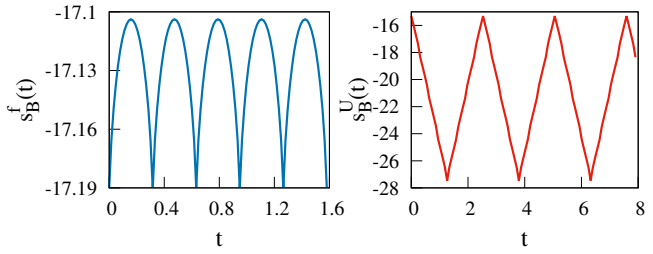

FIG. 12. Plot of $s_B^f(t)$ and $s_B^U(t)$ for the 'atypical' initial configuration and parameters considered in Fig. (11). The periodic oscillation in both cases imply that the system never reaches equilibrium. For the left figure we have used grid size $\Delta x = \Delta v = 0.5$ and for the right figure we have used $\ell = 0.1$.

the exact conservation equation

$$\partial_t e + \partial_x J = 0, \tag{36}$$

$$\text{where} \quad J(x,t) = \frac{1}{2}\int_{-\infty}^{\infty} dv\ v^3 f(x,v,t) \tag{37}$$

is the energy current density. It is instructive to rewrite this equation in the following form:

$$\partial_t e + \partial_x[v(e+P)] = -\partial_x J_s, \tag{38}$$

$$\text{where } J_s(x,t) = J - v(e+P) \tag{39}$$

is the current after subtracting the reversible Euler part. This current, J_s, can be interpreted as a "heat" current. Then, repeating the steps as before we find that the entropy production rate is finite and given by

$$\frac{dS(t)}{dt} = -\int_0^L dx\ \frac{\partial_x J_s}{T} = -\int_0^L dx \frac{J_s \partial_x T}{T^2}, \tag{40}$$

where in the last step we used the fact that the current vanishes at the boundaries. For our system we can compute the fields $J_s(x,t)$ and $T(x,t)$ directly from the exact solution of the microscopic dynamics and thereby compute the entropy production rate from the above equation. In Fig. (10) we compare this with the entropy production rate obtained from the definition given by Eq. (14) and find perfect agreement between the two. However, as shown in the inset of Fig. (10), we find that the integrand is not everywhere non-negative and we are not able to prove analytically that the entropy production rate is non-negative. Note that for generic interacting non-integrable systems, the term J_s should be expressible in terms of the three basic fields and in fact given by the Fourier's law $J_s = -\kappa\partial_x T$. This form would then guarantee non-negativity of the entropy production rate.

We briefly comment on the growth of S_B^f. For the case of our non-interacting gas, Eq. (18) or Eq. (10) are analogous to the Euler equations and the growth of S_B^f was purely a result of the discretization of μ-space. Another well known trivially integrable system is the harmonic chain. The Euler equations for this system were written in [38] where it was also noted that a finite space-time scaling parameter led to a Navier-Stokes type correction term [39]. Interestingly, for the disordered harmonic chain, closed form Euler equations can be written for just the stretch and momentum variables, even though the system has a macroscopic number of conserved quantities [40].

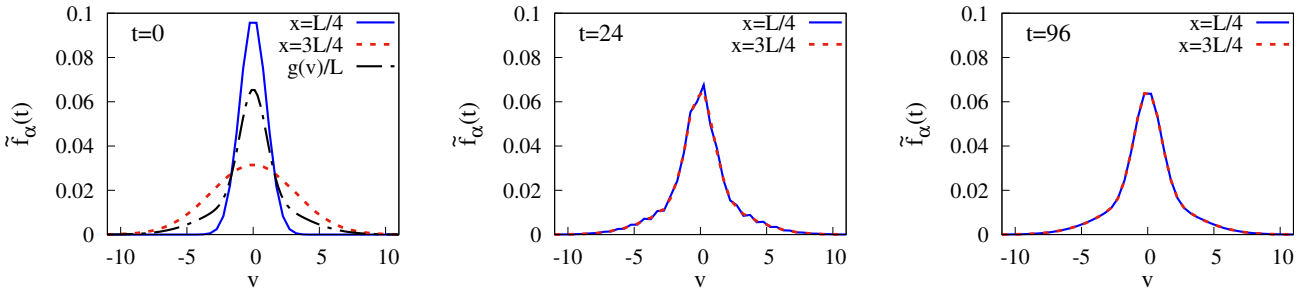

FIG. 13. Plot of evolution of the empirical particle density $\tilde{f}_\alpha(x,v,t) = f_\alpha(x,v,t)/N$, starting from a single two-temperature initial microstate, at two spatial locations $x = L/4$ and $x = 3L/4$. The initial position of $N = 10^7$ particles are distributed uniformly within $(0, L)$ with $L = 4$, while the initial velocities of the particles in the left and right halves are drawn from Maxwell distributions at temperatures $T_L = 1$ and $T_R = 10$, respectively. The grid size was taken as $\Delta x = \Delta v = 0.5$. At $t = 0$ the empirical density $f_\alpha(x,v,t)$ is Maxwellian with $T_0 = 1$ and $T_0 = 10$ at $x = L/4$ and $x = 3L/4$, respectively. As time evolves, the empirical density at any position gets contribution from particles originating initially from both the Maxwell distributions. After a large time, the distribution $\tilde{f}_\alpha(x,v,t)$ is seen to approach the form $g(v)/L$ (shown by the black dash-dot line in the left-most panel), where $g(v) = [g_{\rm eq}(v,1) + g_{\rm eq}(v,10)]/2$ and $g_{\rm eq}(v,T_0)$ is given in Eq. (16).

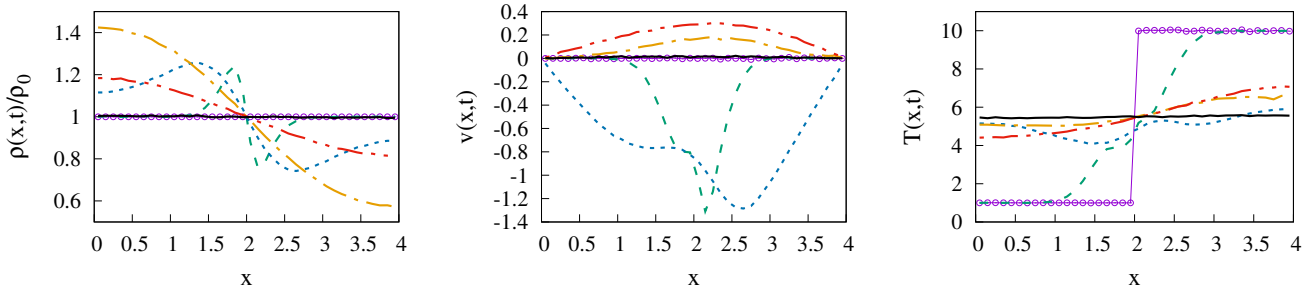

FIG. 14. Plot of the spatial profiles of the three conserved fields density $\rho(x,t)$, velocity $v(x,t)$, and temperature $T(x,t)$ for the 'two-temperature case' at different times $t = 0$ (magenta circles), 0.1 (green dashed lines), 0.4 (blue dotted lines), 1 (yellow dash-dot lines), 2 (red dash-dot-dot lines), and 4 (black solid lines) obtained from simulation of a single initial microscopic configuration with $N = 10^7$ particles. The initial condition is the same as that used in Fig. (13). Notice that after a highly nontrivial evolution, all three profiles become flat and thus the system reaches the equilibrium state at long times.

IV. OTHER INITIAL CONDITIONS

So far we have considered a single typical initial condition for a macrostate in which the initial positions are uniformly distributed in $(0, L/2)$ and the initial velocities are chosen from a (uniform) Maxwell distribution. We found that at large times the system goes to equilibrium, with the profiles of the conserved fields becoming flat and the corresponding entropy $s_B^U(t)$ reaching a steady value. It is also interesting to study the evolution for a single initial condition, atypical for all the particles being on the left side.

To do that we first consider a single configuration of $N = 10^7$ particles initially in the left half $(0, L/2)$ distributed uniformly. The initial velocities of odd particles are set to $v_0 = \sqrt{T_0}$ and that of even particles are set to $v_0 = -\sqrt{T_0}$, with $T_0 = 2.5$. Interestingly, in this case, each particle comes back to its original position with its original velocity periodically after a time period $2L/\sqrt{T_0}$. This recurrence is observed in Fig. (11), where we plot the profiles of the three conserved fields density $\rho(x,t)$, velocity $v(x,t)$, and temperature $T(x,t)$ at different times. We note that the profiles repeat themselves after a time period 8τ with $\tau = L/(4\sqrt{T_0})$. Thus, unlike for the typical initial configuration in Fig. (7), for this atypical initial condition the system never settles down into an equilibrium state for either of our two choices of macrovariables. We have also looked at the evolution of the entropies $s_B^f(t)$ and $s_B^U(t)$ for this atypical initial configuration in Fig. (12), where we find, of course, that the entropy in both cases keeps oscillating for all time.

We also consider another initial microstate corresponding to an f-macrostate (choice-I) where the particles are uniformly distributed over the full box with zero momentum and with two different temperatures on the left and right half of the box, i.e., with the velocities chosen from the corresponding Maxwellians. In Fig. (13) we show the time-evolution of $f(x,v,t)$ while Fig. (14) shows the evolution of the three fields – density, velocity and temperature. In the former case we see that the long-time

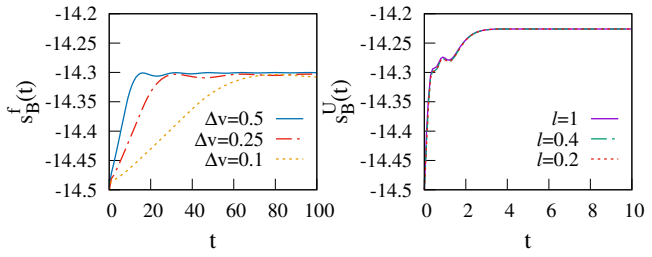

FIG. 15. Plot of $s_B^f(t)$ and $s_B^U(t)$ obtained from simulation of a single realization starting from the two-temperature initial configuration. The initial condition is the same as that used in Fig. (13). We have used several grid sizes for computing s_B^f and s_B^U. While both entropies saturate at large times, only the final value of s_B^U corresponds to the thermodynamic equilibrium value. Since the final velocity distribution at long times is not Maxwellian, the saturation value of s_B^f does not correspond to the equilibrium value. Observe that the growth is non-monotonic in both cases. We also see convergence of s_B^U with coarse-graining scale ℓ while for s_B^f we again see a decreasing growth rate with decreasing Δv.

form of the single particle distribution is non-thermal, i.e. non-Maxwellian, as demonstrated and explained in Fig. (13). On the other hand, the fields $\rho(x,t)$, $v(x,t)$ and $T(x,t)$ are converging to their expected thermal equilibrium values, as shown in Fig. (14). In Fig. (15) we compare the evolution of s_B^f and s_B^U for the case where the left and right halves are initially at temperatures $T_L = 1$ and $T_R = 10$ respectively. We note that both s_B^U and s_B^f saturate at long times but the increase in entropy is less for s_B^f. This is because the conserved fields evolve at long times to their thermodynamic equilibrium values, with uniform density, zero momentum and temperature $T = (T_L + T_R)/2$, with s_B^U thus attaining the corresponding equilibrium value. On the other hand, the total velocity distribution does not evolve with time and hence remains non-Maxwellian at all times. Thus s_B^f saturates to a value lower than the equilibrium one. From Eq. (28) and the discussion in that section we find that the saturation value of s_B^f is given by Eq. (29) with $\bar{g}(v) = [g_{\rm eq}(v,T_L) + g_{\rm eq}(v,T_R)]/2$. This agrees with the measured saturation value in Fig. (15). The invariant velocity distribution $\bar{g}(v)$ which is just the mean of two Maxwellians in fact defines a corresponding generalized Gibbs ensemble (GGE) that describes the long-time equilibrium state of the system. Note that the entropy growth for both definitions of entropy is non-monotonic, unlike what is seen for s_B^U for free expansion.

V. GEOMETRICAL OVERVIEW

Apart from the macrovariables, U, f, let us also define another one, corresponding to the global velocity distribution: $g(v) = \int dx f(x,v)/N$. For the equal mass gas, this is a constant of the motion. Each of U, f and g de-

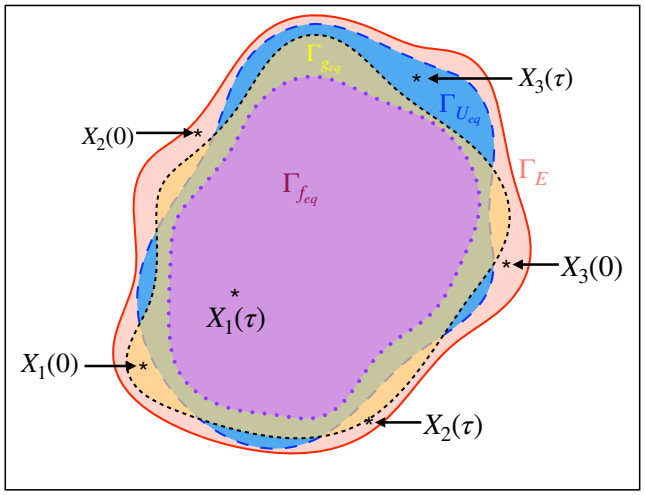

FIG. 16. A schematic showing the partition of the full phase space into subspaces defined by the equilibrium macrostates $f_{\rm eq}$ (boundary shown by dotted-line), $U_{\rm eq}$ (boundary with long-dashed line) and $g_{\rm eq}$ (boundary with dashed line). The points $X_1(0), X_2(0), X_3(0)$ correspond to the three initial microstates considered in our study. The point $X_1(0)$ corresponds to the free expansion from thermal equilibrium, $X_2(0)$ corresponds to free expansion from the alternate velocity microstate and $X_3(0)$ corresponds to the uniform density non-Maxwellian (two-temperature) initial global velocity distribution. After a long time, τ, these microstates, $X_1(\tau), X_2(\tau), X_3(\tau)$, would remain in regions of phase space as shown in the figure (making brief excursions out of these regions on Poincare recurrence time-scales). We note that $X_1(\tau)$ will be contained in $\Gamma_{f_{\rm eq}}$, $X_2(\tau)$ is outside $\Gamma_{f_{\rm eq}} \cup \Gamma_{U_{\rm eq}} \cup \Gamma_{g_{\rm eq}}$, and $X_3(\tau)$ will end up in $\Gamma_{U_{\rm eq}} \setminus \Gamma_{f_{\rm eq}}$ (all points in $\Gamma_{U_{\rm eq}}$ that are not in $\Gamma_{f_{\rm eq}}$).

fine partitions of Γ_E : $\Gamma_E = \{\Gamma_U\} = \{\Gamma_f\} = \{\Gamma_g\}$, where $\{...\}$ represents the collection of all possible macrostate values. The last, $\{\Gamma_g\}$, is a partition of Γ_E into sets invariant under the dynamics. Each of the three partitions has a dominant set, $\Gamma_{U_{\rm eq}}$, $\Gamma_{f_{\rm eq}}$, and $\Gamma_{g_{\rm eq}}$, respectively. These are shown schematically in Fig. (16). The macrostate $U_{\rm eq}$ corresponds to uniform profiles of the conserved fields, $f_{\rm eq}$ corresponds to a macrostate with uniform density profile and Maxwellian velocity distribution, and $g_{\rm eq}$ corresponds to a global Maxwellian velocity distribution. Note that the f partition of Γ_E is a refinement of the U partition and also a refinement of the g partition.

As shown in the figure, $\Gamma_{f_{\rm eq}}$ is the dominant set in $\Gamma_{U_{\rm eq}}$ and in $\Gamma_{g_{\rm eq}}$, while $\Gamma_{g_{\rm eq}}$ has tiny regions that are outside $\Gamma_{U_{\rm eq}}$ and vice-versa. Any initial microstate, $X_1(0)$, inside $\Gamma_{g_{\rm eq}}$, such as the one chosen from thermal equilibrium in the left half of the box, will eventually be in the region $\Gamma_{f_{\rm eq}} \cap \Gamma_{U_{\rm eq}} \cap \Gamma_{g_{\rm eq}} = \Gamma_{f_{\rm eq}}$ which corresponds to "complete" thermal equilibrium. On the other hand typical microstates such as $X_3(0)$, chosen from outside of $\Gamma_{g_{\rm eq}}$ will end in $\Gamma_{U_{\rm eq}}$ but outside $\Gamma_{f_{\rm eq}}$ and so in this case we have restricted thermalization. This is seen in

Fig. (15) where s_B^U is seen to reach its equilibrium value while s_B^f does not. Finally one has very special atypical microstates, $X_2(0)$, such as in the alternate velocity case considered in Fig. (12), which remains outside $\Gamma_{f_{\rm eq}} \cup \Gamma_{U_{\rm eq}} \cup \Gamma_{g_{\rm eq}}$ and there is no thermalization at all. The above features are specific to our system, a non-interacting integrable model. For non-integrable models it is expected that almost any initial microstate would end in $\Gamma_{f_{\rm eq}}$ and the system would thermalize completely.

VI. CONCLUSION

We summarize here our main findings. In this paper, we have studied entropy increase during the free expansion of an ideal gas. In the microscopic description we start from an initial condition where the molecules are uniformly distributed in the left half of a box and the velocities are chosen from a thermal distribution. For this system we study the evolution of the Boltzmann entropy defined for a single microstate with two choices of macrovariables: the empirical single particle distribution $f(x, v, t)$ and the profiles of density, momentum and energy $U = [\rho(x), p(x), e(x)]$ (or equivalently ρ, v, T). The corresponding entropies are s_B^f and s_B^U, respectively. In equilibrium, both these choices correspond to the thermodynamic entropy S.

- The time evolution of the empirical density $f(x, v, t)$ and the fields $\rho(x, t), v(x, t), T(x, t)$ were obtained for a single realization, starting from a single typical initial microstate chosen from the equilibrium macrostate where all particles are in equilibrium in the left half of a box. We found that these agree, in the large N limit, with the corresponding fields $F_\alpha, \bar{\rho}, \bar{v}, \bar{T}$, obtained by *averaging* over initial microstates taken from the relevant initial Gibbs distribution or, more or less equivalently, from the same initial macrostate. For our model, the averaged fields can easily be computed exactly. This demonstrates that the evolution of the macrostates and the corresponding entropies, for single typical microstates (belonging to a macrostate $M_{\rm ini}$), agrees with the evolution obtained after averaging over the ensemble of initial conditions (corresponding to the same initial macrostate $M_{\rm ini}$).

- Both s_B^f and s_B^U increase with time and eventually reach the expected equilibrium value with an increase of $\ln(2)$ per particle. However, while s_B^U increases monotonically with time, s_B^f shows oscillations which decay with time.

- The entropies are defined in terms of coarse graining scales $|\Delta_\alpha|$ for s_B^f and ℓ for s_B^U. We find that the entropy production rate for s_B^U does not depend much on decreasing grid-size ℓ. On the other hand, s_B^f decreases with decreasing Δv. However, we find a remarkable scaling collapse of the data for $s_B^f(t)$ for different Δv on plotting them as a function of the scaled time $\tau = t\Delta v/(2L)$. We provide an analytic understanding of this collapse and compute the scaling function. This also explains the oscillations and in particular the observation that the system periodically goes to the maximum entropy state.

- We showed that the entropy increase for S_B^U can be related to a microscopic "heat" current, J_s, and formally the local entropy production rate can be written in the form $J_s \partial_x(1/T)$. However, we find that this is not positive-definite (as expected for non-integrable systems with heat diffusion). Nevertheless, the integral over all space gives a positive entropy production.

- **Other initial conditions**: The results above are for the specific case of free expansion. We have also studied other initial conditions. We considered one example (with an atypical initial microstate with alternate particles having different velocities, $\pm v_0$) where the system never reaches a steady state and the entropy shows persistent oscillations. Our second example involves particles initially distributed uniformly in the box but with a non-Maxwellian global velocity distribution. For this case we find that s_B^U saturates to its equilibrium value at long times, while s_B^f does not, corresponding to the observed fact that the macrovariables f and U evolve in this case to limiting values: U evolves to its equilibrium value $U_{\rm eq}$ while f evolves to g/L, corresponding to the dominant f-macrostate given the total velocity distribution arising from $f_{\rm initial}$.

Thus our study illustrates the crucial role of typicality, large numbers and coarse-grainingthat lead to entropy increase, irreversibility and approach to thermal equilibrium, even in a non-interacting integrable system. The ideas of ergodicity, interaction and chaos do not seem to be so relevant.

Thermalization in non-chaotic systems, such as the Toda chain, has been discussed in other recent papers [41, 42]. The one-dimensinal hard rod gas, an integrable model which however has a Navier-Stokes term in the hydrodynamic equations [27], would be another interesting case to study from the present perspective. It will also be interesting to extend the study of the present paper to interacting systems such as the alternate mass hard particle gas where the masses of alternate particles take different values. This non-integrable model has been studied extensively in the context of the breakdown of Fourier's law of heat conduction in one dimension [43–46] and verification of the hydrodynamic description [47–50]. For this case we expect important differences from the present integrable model even though the equilibrium thermodynamics of both are identical. For example we expect that the entropy production rate for s_B^f at a fixed time should converge to a finite positive value even in the

limit of vanishing grid-size, in contrast to what we see in Fig. (2). Another difference is that we expect is that the heat current term, J_s, in Eq. (39) should be given by a diffusive term leading to positive entropy production rate at the local level (in contrast to the inset in Fig. (10)).

ACKNOWLEDGMENTS

SC, AD and AK acknowledge support of the Department of Atomic Energy, Government of India, under Project No. RTI4001 and would also like to acknowledge the ICTS program on "Thermalization, Many body localization and Hydrodynamics (Code:ICTS/hydrodynamics2019/11)" for enabling crucial discussions related to this work. SC, AD and AK thank Cedric Bernardin, Deepak Dhar, Francois Huveneers, Christian Maes, Stefano Olla, and Herbert Spohn for illuminating discussions. We thank Cedric Bernardin, Vir Bulchandani, Benjamin Doyon, David Huse and Joel Moore for helpful comments on the manuscript. The work of JLL was supported by the AFOSR. The numerical simulations were performed on a Mario HPC at ICTS-TIFR.

[1] L. Boltzmann, On Zermelo's paper "On the mechanical explanation of irreversible processes", Annalen der Physik **60**, 392 (1897).
[2] R. Feynman, *The character of physical law* (MIT press, 2017).
[3] O. E. Lanford, On a derivation of the Boltzmann equation, Astérisque **40**, 117 (1976).
[4] R. Penrose, *The Emperor's New Mind: Concerning Computers, Minds, and the Laws of Physics* (Oxford University Press, Inc., USA, 1989).
[5] B. Greene, *The fabric of the cosmos: Space, time, and the texture of reality* (Knopf, 2004).
[6] J. L. Lebowitz, Macroscopic laws, microscopic dynamics, time's arrow and Boltzmann's entropy, Physica A **194**, 1 (1993).
[7] J. L. Lebowitz, Boltzmann's entropy and time's arrow, Physics Today **46**, 32 (1993).
[8] J. L. Lebowitz, From time-symmetric microscopic dynamics to time-asymmetric macroscopic behavior: An overview, in *Boltzmann's Legacy (ESI Lectures in Mathematics and Physics)*, edited by G. Gallavotti, W. L. Reiter, and J. Yngvason (European Mathematical Society, 2008) p. 63, arXiv:0709.0724 [cond-mat.stat-mech].
[9] S. Goldstein, J. L. Lebowitz, R. Tumulka, and N. Zanghì, Gibbs and Boltzmann entropy in classical and quantum mechanics, in *Statistical Mechanics and Scientific Explanation: Determinism, Indeterminism and Laws of Nature*, edited by V. Allori (World Scientific, Singapore, 2020) Chap. 14, p. 519, arXiv:1903.11870 [cond-mat.stat-mech].
[10] J. L. Lebowitz, Statistical mechanical ensembles and typical behavior of macroscopic systems, (Talk at ICTS, 2021).
[11] B. J. Alder and T. E. Wainwright, *Proceedings of the International Symposium on Transport Processes in Statistical Mechanics Held in Brussels, August 27-31, 1956*, edited by I. Prigogine (Interscience Publishers, 1958).
[12] J. Orban and A. Bellemans, Velocity-inversion and irreversibility in a dilute gas of hard disks, Phys. Lett. A **24**, 620 (1967).
[13] D. Levesque and L. Verlet, Molecular dynamics and time reversibility, J. Stat. Phys. **72**, 519 (1993).
[14] V. Romero-Rochín and E. González-Tovar, Comments on some aspects of Boltzmann H theorem using reversible molecular dynamics, J. Stat. Phys. **89**, 735 (1997).
[15] M. Falcioni, L. Palatella, S. Pigolotti, L. Rondoni, and A. Vulpiani, Initial growth of Boltzmann entropy and chaos in a large assembly of weakly interacting systems, Physica A **385**, 170 (2007).
[16] E. T. Jaynes, Violation of Boltzmann's H theorem in real gases, Phys. Rev. A **4**, 747 (1971).
[17] S. Goldstein and J. L. Lebowitz, On the (Boltzmann) entropy of non-equilibrium systems, Physica D **193**, 53 (2004).
[18] P. L. Garrido, S. Goldstein, and J. L. Lebowitz, Boltzmann entropy for dense fluids not in local equilibrium, Phys. Rev. Lett. **92**, 050602 (2004).
[19] H. L. Frisch, Poincaré recurrences, Phys. Rev. **104**, 1 (1956).
[20] D. Jepsen, Dynamics of a simple many-body system of hard rods, J. Math. Phys. **6**, 405 (1965).
[21] J. L. Lebowitz and J. K. Percus, Kinetic equations and density expansions: Exactly solvable one-dimensional system, Phys. Rev. **155**, 122 (1967).
[22] J. L. Lebowitz, J. K. Percus, and J. Sykes, Time evolution of the total distribution function of a one-dimensional system of hard rods, Phys. Rev. **171**, 224 (1968).
[23] J. K. Percus, Exact solution of kinetics of a model classical fluid, The Physics of Fluids **12**, 1560 (1969).
[24] A. Roy, O. Narayan, A. Dhar, and S. Sabhapandit, Tagged particle diffusion in one-dimensional gas with hamiltonian dynamics, J. Stat. Phys. **150**, 851 (2013).
[25] A. Kundu and A. Dhar, Equilibrium dynamical correlations in the toda chain and other integrable models, Phys. Rev. E **94**, 062130 (2016).
[26] C. Boldrighini, R. L. Dobrushin, and Y. M. Sukhov, One-dimensional hard rod caricature of hydrodynamics, J. Stat. Phys. **31**, 577 (1983).
[27] B. Doyon and H. Spohn, Dynamics of hard rods with initial domain wall state, J. Stat. Mech. **2017**, 073210 (2017).
[28] X. Cao, V. B. Bulchandani, and J. E. Moore, Incomplete thermalization from trap-induced integrability breaking: Lessons from classical hard rods, Phys. Rev. Lett. **120**, 164101 (2018).
[29] H. Tasaki, Typicality of thermal equilibrium and thermalization in isolated macroscopic quantum systems, J. Stat. Phys. **163**, 937 (2016).
[30] T. Mori, T. N. Ikeda, E. Kaminishi, and M. Ueda, Thermalization and prethermalization in isolated quantum systems: a theoretical overview, J. Phys. B **51**, 112001 (2018).
[31] S. Goldstein, Individualist and ensemblist approaches to the foundations of statistical mechanics, The Monist **102**,

439 (2019).
[32] S. Goldstein, D. A. Huse, J. L. Lebowitz, and R. Tumulka, Macroscopic and microscopic thermal equilibrium, Annalen der Physik **529**, 1600301 (2017).
[33] S. Goldstein, D. A. Huse, J. L. Lebowitz, and P. Sartori, On the nonequilibrium entropy of large and small systems, in *Stochastic Dynamics Out of Equilibrium (IHPStochDyn 2017: Stochastic Dynamics Out of Equilibrium)*, Vol. 282, edited by G. Giacomin, S. Olla, E. Saada, H. Spohn, and G. Stoltz (Springer, Berlin, 2019) Chap. 22, p. 581, arXiv:1712.08961 [cond-mat.stat-mech].
[34] S. Goldstein, Boltzmann's approach to statistical mechanics, in *Chance in Physics: Foundations and Perspectives (Lecture Notes in Physics)*, Vol. 574, edited by J. Bricmont, G. Ghirardi, D. Dürr, F. Petruccione, M. C. Galavotti, and N. Zanghì (Springer, Berlin, 2001) Chap. 3, p. 39, arXiv:0105242 [cond-mat.stat-mech].
[35] O. Penrose, *Foundations of statistical mechanics: a deductive treatment* (Dover, 2005).
[36] Y. Oono, *Perspectives on Statistical Thermodynamics* (Cambridge University Press, 2017).
[37] C. Cercignani, R. Illner, and M. Pulvirenti, *The mathematical theory of dilute gases*, Vol. 106 (Springer Science & Business Media, 2013).
[38] R. Dobrushin, A. Pellegrinotti, Y. M. Suhov, and L. Triolo, One-dimensional harmonic lattice caricature of hydrodynamics, J. Stat. Phys. **43**, 571 (1986).
[39] R. Dobrushin, A. Pellegrinotti, Y. M. Suhov, and L. Triolo, One-dimensional harmonic lattice caricature of hydrodynamics: second approximation, J. Stat. Phys. **52**, 423 (1988).
[40] C. Bernardin, F. Huveneers, and S. Olla, Hydrodynamic limit for a disordered harmonic chain, Communications in Mathematical Physics **365**, 215 (2019).
[41] M. Baldovin, A. Vulpiani, and G. Gradenigo, Statistical mechanics of an integrable system, J. Stat. Phys. **183**, 1 (2021).
[42] S. Ganapa, A. Apte, and A. Dhar, Thermalization of local observables in the α-FPUT chain, J. Stat. Phys. **180**, 1010 (2020).
[43] A. Dhar, Heat conduction in a one-dimensional gas of elastically colliding particles of unequal masses, Phys. Rev. Lett. **86**, 3554 (2001).
[44] P. Grassberger, W. Nadler, and L. Yang, Heat conduction and entropy production in a one-dimensional hard-particle gas, Phys. Rev. Lett. **89**, 180601 (2002).
[45] G. Casati and T. Prosen, Anomalous heat conduction in a one-dimensional ideal gas, Phys. Rev. E **67**, 015203 (2003).
[46] P. Cipriani, S. Denisov, and A. Politi, From anomalous energy diffusion to levy walks and heat conductivity in one-dimensional systems, Phys. Rev. Lett. **94**, 244301 (2005).
[47] H. Spohn, Nonlinear fluctuating hydrodynamics for anharmonic chains, J. Stat. Phys. **154**, 1191 (2014).
[48] C. B. Mendl and H. Spohn, Shocks, rarefaction waves, and current fluctuations for anharmonic chains, J. Stat. Phys. **166**, 841 (2016).
[49] S. Chakraborti, S. Ganapa, P. L. Krapivsky, and A. Dhar, Blast in a one-dimensional cold gas: From newtonian dynamics to hydrodynamics, Phys. Rev. Lett. **126**, 244503 (2021).
[50] S. Ganapa, S. Chakraborti, P. Krapivsky, and A. Dhar, Blast in the one-dimensional cold gas: Comparison of microscopic simulations with hydrodynamic predictions, Physics of Fluids **33**, 087113 (2021).
[51] H. L. Frisch, An approach to equilibrium, Phys. Rev. **109**, 22 (1958).

Appendix A: Exact solution for the evolution of macroscopic fields

Here we present exact results for the evolution of average fields corresponding to the empirical densities $f(x,p,t)$ and $[\rho(x,t),p(x,t),e(x,t)]$. A similar study on a ring was done earlier in [51].

The mean density $\bar{\rho}(x,t)$, momentum $\bar{p}(x,t)$ and energy $\bar{e}(x,t)$ fields are defined as

$$\bar{\rho}(x,t) = \left\langle \sum_{j=1}^{N} \delta(x_j - x) \right\rangle = \int dv\ F(x,v,t), \tag{A1}$$

$$\bar{p}(x,t) = \left\langle \sum_{j=1}^{N} \delta(x_j - x) v_j \right\rangle = \int dv\ v\ F(x,v,t), \tag{A2}$$

$$\bar{e}(x,t) = \left\langle \sum_{j=1}^{N} \delta(x_j - x) \frac{v_j^2}{2} \right\rangle = \int dv\ \frac{v^2}{2}\ F(x,v,t). \tag{A3}$$

Here $\langle ... \rangle$ denotes an average over the initial positions and velocities, $\{x_i(0), v_i(0)\}$, of all the particles, which are chosen from the canonical distribution at temperature T with all particles in the left half $(0, L/2)$. In the following, we study the evolution of these fields in time and space for this system with two reflecting boundaries at $x = 0$ and $x = L$.

The canonical ensemble implies that we distribute the particles uniformly in $(0, L/2)$ and draw their velocities from the Maxwell's velocity distribution given by

$$g_{\rm eq}(v_0, T) = \left(\frac{1}{2\pi T}\right)^{1/2} \exp\left[\frac{-v_0^2}{2T}\right]. \tag{A4}$$

As discussed earlier, we can effectively treat the particles as non-interacting and the problem reduces to a single particle problem [24]. We then consider a single particle starting from an initial position x_0 with initial velocity v_0. The final position, x_t, of the particle, taking all possible collisions into account, can take the following forms:

$$x_t = \begin{cases} x_0 + v_0 t - 2nL, & \text{if } \ v_0 > 0, v_t > 0, \\ x_0 + v_0 t + 2nL, & \text{if } \ v_0 < 0, v_t < 0, \\ -x_0 - v_0 t + 2nL, & \text{if } \ v_0 > 0, v_t < 0, \\ -x_0 - v_0 t - 2nL, & \text{if } \ v_0 < 0, v_t > 0, \end{cases} \tag{A5}$$

where v_t, the velocity at time t, can take either values $\pm v_0$ and $n = 0, 1, 2, 3...$, is the number of collision(s) that the particle has with both the boundaries. The distribution $F(x,v,t)$ is then obtained by averaging over the initial

position [uniform in $(0, L/2)$] and velocity [drawn from $g_{\rm eq}(v_0, T)$]:

$$F(x, v, t) = N\langle \delta(x - x_t)\delta(v - v_t)\rangle. \tag{A6}$$

Using Eq. (A5) we get:

$$F(x,v,t) = \frac{2N}{L}\int_0^{L/2} dx_0 \int_{-\infty}^{\infty} dv_0 g_{\rm eq}(v_0) \sum_{n=-\infty}^{\infty} \left[\delta(x - x_0 - v_0 t + 2nL)\delta(v - v_0) + \delta(x + x_0 + v_0 t - 2nL)\delta(v + v_0)\right], \tag{A7}$$

$$= 2\rho_0 \frac{\exp(-v^2/2T)}{\sqrt{2\pi T}} \sum_{n=-\infty}^{\infty} [\Theta(x - vt - 2nL + L/2) - \Theta(x - vt + 2nL - L/2)], \tag{A8}$$

where $\rho_0 = N/L$. Now we calculate the three mean fields by performing the integrals in Eqs. (A1), (A2), and (A3) to get

$$\begin{aligned}
\bar{\rho}(x,t) &= \int_{-\infty}^{\infty} dv F(x,v,t), \\
&= 2\rho_0 \frac{1}{\sqrt{2\pi T}} \sum_{n=-\infty}^{\infty} \int_0^{L/2} dx_0 \int_{-\infty}^{\infty} dv\ e^{-v^2/2T} \left[\delta(x - x_0 - vt + 2nL) + \delta(x + x_0 - vt - 2nL)\right], \\
&= 2\rho_0 \frac{1}{\sqrt{2\pi T}} \sum_{n=-\infty}^{\infty} \int_0^{L/2} dx_0 \frac{1}{t}\left[\exp\left\{\frac{-(2nL + x - x_0)^2}{2Tt^2}\right\} + \exp\left\{\frac{-(2nL - x - x_0)^2}{2Tt^2}\right\}\right], \\
&= \rho_0 \sum_{n=-\infty}^{\infty} \left[\mathrm{erf}\left(\frac{L/2 - 2nL - x}{\sqrt{2T}t}\right) + \mathrm{erf}\left(\frac{L/2 - 2nL + x}{\sqrt{2T}t}\right)\right].
\end{aligned} \tag{A9}$$

Using the Poisson resummation formula, this can be rewritten in the alternative series form:

$$\bar{\rho}(x,t) = \rho_0 + 4\rho_0 \sum_{k=1}^{\infty} \frac{1}{k\pi} \sin\left(\frac{k\pi}{2}\right) \cos\left(\frac{k\pi x}{L}\right) \exp\left(\frac{-k^2\pi^2 T t^2}{2L^2}\right). \tag{A10}$$

Following a similar approach we obtain the following expressions for the mean momentum and energy:

$$\begin{aligned}
\bar{p}(x,t) &= \int_{-\infty}^{\infty} dv\ v F(x,v,t), \\
&= \rho_0 \sqrt{\frac{2T}{\pi}} \sum_{n=-\infty}^{\infty} \left[\exp\left\{-\frac{(2nL - L/2 + x)^2}{2Tt^2}\right\} - \exp\left\{-\frac{(2nL - L/2 - x)^2}{2Tt^2}\right\}\right], \qquad \text{(A11)} \\
&= \frac{4\rho_0 T t}{L} \sum_{k=1}^{\infty} \sin\left(\frac{k\pi}{2}\right) \sin\left(\frac{k\pi x}{L}\right) \exp\left(\frac{-k^2\pi^2 T t^2}{2L^2}\right), \qquad \text{(A12)} \\
\bar{e}(x,t) &= \frac{1}{2}\int_{-\infty}^{\infty} dv\ v^2 F(x,v,t), \\
&= \rho_0 \frac{2T}{\sqrt{\pi}} \sum_{n=-\infty}^{\infty} \left[-\frac{\sqrt{\pi}}{4}\mathrm{erf}\left(\frac{2nL - L/2 + x}{\sqrt{2T}t}\right) + \frac{2nL - L/2 + x}{2\sqrt{2T}t} \exp\left\{\frac{-(2nL - L/2 + x)^2}{2Tt^2}\right\}\right. \\
&\left. -\frac{\sqrt{\pi}}{4}\mathrm{erf}\left(\frac{2nL - L/2 - x}{\sqrt{2T}t}\right) + \frac{2nL - L/2 - x}{2\sqrt{2T}t} \exp\left\{\frac{-(2nL - L/2 - x)^2}{2Tt^2}\right\}\right]. \qquad \text{(A13)} \\
&= \frac{\rho_0 T}{2} + 2\rho_0 T \sum_{k=1}^{\infty} \frac{1}{k\pi}\left(1 - \frac{k^2\pi^2 T t^2}{L^2}\right) \sin\left(\frac{k\pi}{2}\right) \cos\left(\frac{k\pi x}{L}\right) \exp\left(\frac{-k^2\pi^2 T t^2}{2L^2}\right). \qquad \text{(A14)}
\end{aligned}$$

From Eqs. (A10, A12, A14) one can easily see that the approach to equilibrium has the long-time form e^{-at^2} with $a = T\pi^2/(2L^2)$.